VOL. 288 NO. 10 OCTOBER 2006

The Anatomical Record

PART A: Discoveries in molecular, cellular, and evolutionary biology

AN OFFICIAL PUBLICATION OF THE AMERICAN ASSOCIATION OF ANATOMISTS • KURT H. ALBERTINE • EDITOR-IN-CHIEF

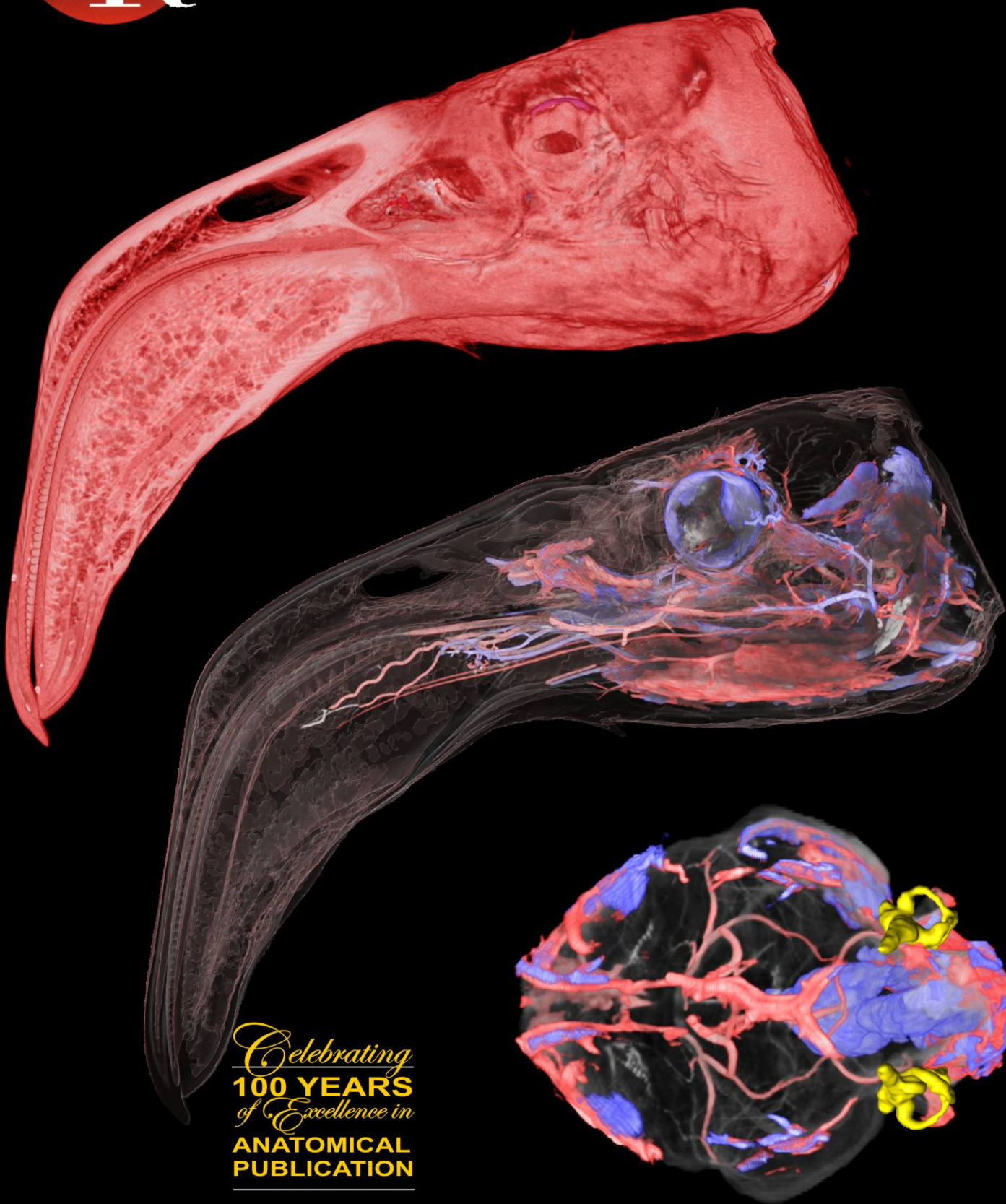

Celebrating
100 YEARS
of Excellence in
ANATOMICAL
PUBLICATION

Cephalic Vascular Anatomy in Flamingos (*Phoenicopterus ruber*) Based on Novel Vascular Injection and Computed Tomographic Imaging Analyses

CASEY M. HOLLIDAY,[1,2] RYAN C. RIDGELY,[2] AMY M. BALANOFF,[3] AND LAWRENCE M. WITMER[2*]

[1]Department of Biological Sciences, Ohio University, Athens, Ohio
[2]Department of Biomedical Sciences, College of Osteopathic Medicine, Ohio University, Athens, Ohio
[3]High Resolution X-Ray CT Facility, Department of Geological Sciences, University of Texas, Austin, Texas

ABSTRACT

Head vascular anatomy of the greater (or Caribbean) flamingo (*Phoenicopterus ruber*) is investigated and illustrated through the use of a differential contrast, dual vascular injection technique, and high-resolution X-ray computed tomography (CT), allowing arteries and veins to be differentiated radiographically. Vessels were digitally isolated with segmentation

Abbreviations used: aAD, arteria alveolar dorsalis; aBA, arteria basilaris; aCA, arteria cerebralis caudalis; aCC, arteria carotis communis; aCE, arteria cerebralis caudalis; aCF, arteria cerebralis frontalis; aCI, arteria carotis interna; aCL, arteria cerebralis lateralis; aCM, arteria cerebralis media; aCO, arteria carotis; aCR, arteria cerebralis rostralis; aCY, arteria ciliaris; aEC, arteria encephalica communis; aED, arteria esophagus descendens; aET, arteria ethmoidalis; aEU, arteria encephalica caudalis; aFA, arteria facialis; aFL, arteria flocculus; aFR, arteria frontalis; aHC, arteria hyoideus caudalis; aIO, arteria infraorbitalis; aJU, arteria jugalis; aLA, arteria lacrimalis; aLI, arteria lingualis; aMM, arteria maxillomandibularis; aMN, arteria mandibularis; anCO, anastomosis carotis; anJG, anastomosis interjugularis; aNL, arteria nasalis lateralis; aOC, arteria occipitalis; aOM, arteria orbitalis medialis; aOT, arteria ophthalmotemporalis; aPL, arteria palatina lateralis; aPM, arteria palatina medialis; aPP, arteria pterygopalatina; aPR, arteria profunda; aRC, arteria rostralis communis; aRI, arteria rictalis; aSE, arteria septa nasi; aSL, arteria sublingualis; aSM, arteria submandibularis; aSO, arteria supraorbitalis; aSP, arteria sphenopalatina; aST, arteria stapedia; aTS, arteria temporalis superficialis; aVE, arteria vertebralis; aVR, arteria valleculae rostralis; cCA, concha nasalis caudalis; ch, choana; chr, choroidea; cm, carina maxillaris; cME, concha nasalis media; cSA, canalis semicircularis anterior; cSL, canalis semicircularis lateralis; cSP, canalis semicircularis posterior; cTY, cavum tympanicum; dMN, diverticulum mandibulare; dMX, diverticulum maxillare; fc, fenestra cochleae; fHY, fossa hypophysialis; fMM, fossa mandibularis medialis; fTR, fossa tympanicum rostralis; gLA, glandula lacrimalis; gMN, glandula membranae nictitantis (Harderian gland); gN, glandula nasalis; la, lagena; li, lingua; lJM, ligamentum jugomandibulare; lQM, ligamentum quadratomandibulare; lRO, lamellae rostri; mAMP, musculus adductor mandibulae posterior; mAMEP, musculus adductor mandibulae externus profundus; mAMES, musculus adductor mandibulae externus superficialis; mDM, musculus depressor mandibulae; mea, meatus acusticus externus; mna, meatus nasalis; mPSTS, musculus pseudotemporalis superficialis; mPSTP, musculus pseudotemporalis profundus; mPTD, musculus pterygoideus dorsalis; mPTV, musculus pterygoideus ventralis; mSH, musculus serpihyoideus; na, naris; nAO, nervus anguli oris; nC1, nervus spinalis 1; nMN, nervus mandibularis; nMX, nervus maxillaris; nVA, nervus vagus; oBA, os basihyale; oCH, os ceratohyale; oLA, os lacrimale; oMN, os mandibulare; oPS, os parasphenoidale; oQU, os quadratum; oUR, os urohyale; ph, pharynx; plCC, plexus concha caudalis; plCH, plexus concha; plPA, plexus palatinus; pPO, processus postorbitalis; pRA, processus retroarticularis; rOP, rete ophthalmicum; sAO, sinus antorbitalis; sBA, sinus basilaris; scl, sclera; sPC, sinus paralingualis caudolateralis; sPR, sinus paralingualis rostromedialis; sOC, sinus occipitalis; sSO, sinus suborbitalis; tr, trachea; vCR, vena cephalica rostralis; vJG, vena jugularis; vJI, vena jugularis interna; vLA, vena laryngea; vLI, vena lingualis; vMM, vena maxillomandibularis; vMX, vena maxillaris; vNA, vena nasalis; vOC, vena occipitalis communis; vOP, vena ophthalmica; vPA, vena palatina.

Grant sponsor: National Science Foundation; Grant numbers: NSF IBN-0343744, NSF IOB-0517257 (to L.M.W.).

Amy M. Balanoff's current address is American Museum of Natural History, Division of Paleontology, New York, New York.

*Correspondence to: Lawrence M. Witmer, Department of Biomedical Sciences, College of Osteopathic Medicine, Ohio University, Athens, OH 45701. Fax: 740-593-2400.
E-mail: witmerL@ohio.edu

Received 30 November 2005; Accepted 12 July 2006

DOI 10.1002/ar.a.20374
Published online 8 September 2006 in Wiley InterScience (www.interscience.wiley.com).

tools and reconstructed in 3D to facilitate topographical visualization of the cephalic vascular tree. Major vessels of the temporal, orbital, pharyngeal, and encephalic regions are described and illustrated, which confirm that the general pattern of avian cephalic vasculature is evolutionarily conservative. In addition to numerous arteriovenous vascular devices, a previously undescribed, large, bilateral, paralingual cavernous sinus that excavates a large bony fossa on the medial surface of the mandible was identified. Despite the otherwise conservative vascular pattern, this paralingual sinus was found only in species of flamingo and is not known otherwise in birds. The paralingual sinus remains functionally enigmatic, but a mechanical role in association with the peculiar lingual-pumping mode of feeding in flamingos is perhaps the most likely hypothesis. Anat Rec Part A, 288A:1031–1041, 2006.

Key words: flamingo; vasculature; gross anatomy; stereoangiography; computed tomography; feeding

Aspects of the cephalic vascular system have been studied in a handful of bird species, including domestic chickens (*Gallus gallus*) (Kaku, 1959; Richards, 1967, 1968; Baumel, 1975), herring gulls (*Larus argentatus*) (Midtgård, 1984b), helmeted guinea fowl (*Numida meleagris*) (Crowe and Crowe, 1979), turkey vultures (*Cathartes aura*) (Arad et al., 1989), and mallard ducks (*Anas platyrhynchos*) (Arad et al., 1987; Sedlmayr, 2002). From what is known from the available sample, avian cephalic vasculature appears generally conservative (Baumel, 1993; Sedlmayr, 2002). However, little is known about the head vessels of flamingos, a conspicuously apomorphic bird with a highly divergent feeding apparatus. The greater (or Caribbean) flamingo, *Phoenicopterus ruber*, is one of five species of extant Phoenicopteridae, an avian group most recently allied to Podicipedidae (van Tuinen et al., 2001; Mayr and Clarke, 2003; Mayr, 2004), although relationships with Anseriformes (Feduccia 1976, 1978; Olsen and Feduccia, 1980; Hagey et al., 1990) and Ciconiiformes (Sibley and Ahlquist, 1990) also have been proposed.

Perhaps the most divergent aspect of flamingo natural history is their feeding behavior, during which they invert their heads, holding their extremely ventroflexed bills near horizontal to strain shallow waters for food items such as algae, small invertebrates, and fish. Flamingos separate food items from water and unwanted particles using a large, fatty, highly sensitive tongue with numerous fleshy spines complemented by a keeled, lamellate bill. In general, the tongue is used as a rostrocaudally oriented pump that quickly (5–20 beats/min) sucks in particulate-laden water and expels unwanted solutes via a complex set of movements (Jenkin, 1957; Zweers et al., 1995). Food is then ingested using the typical inertial throw-and-catch behavior of most birds (Zweers et al., 1994). Whereas *P. ruber* has a rather small maxillary keel, other flamingos have more heavily keeled maxillae (Mascitti and Kravetz, 2002). This keel aids in the mediolateral movement of water and solutes toward the lamellate margins of the tongue and bill.

We report here on the general vascular anatomy as well as a novel vascular structure of the flamingo head that potentially relates to this unusual feeding apparatus based on vascular injection, high-resolution CT imaging, three-dimensional digital reconstruction, and gross dissection.

MATERIALS AND METHODS

An adult male specimen of *Phoenicopterus ruber* [Ohio University Vertebrate Collections (OUVC) 9756] was donated to Ohio University from the Brevard Zoo, Melbourne, Florida. The specimen, which died of natural causes unrelated to the system under study here, was frozen very shortly after death and subsequently thawed for study. The specimen was in excellent condition, showing no signs of putrefaction, postmortem coagulation, or freezing artifacts. To promote visualization in dissection and CT scanning, the cephalic blood vascular system was injected with a barium/latex medium using a technique modified from Sedlmayr and Witmer (2002). Although it would have been optimal to have had completely fresh, unfrozen material, such was not possible in that the specimen was not sacrificed for the purpose of this study. Our team, however, has done literally dozens of vascular injections on very similar fresh-frozen specimens with excellent results (Witmer, 2001; Sedlmayr, 2002; Sedlmayr and Witmer, 2002; Clifford and Witmer, 2004; Holliday, 2006). The common carotid artery (aCC; Fig. 1A) and jugular vein (vJG; Figs. 1F and 2) were isolated in dissection and separately cannulated, and the vessels were flushed with tap water for 10 min. Separate 60 cc volumes of both blue and red (Fig. 1E and F) latex injection solution (Ward's, Rochester, NY) were each mixed with Liquid Polibar Plus barium sulfate suspension ($BaSO_4$; E-Z-Em, Westbury, NY) to an approximately 30% barium solution for arteries and 40% barium solution for veins. Different barium concentrations were used to provide a distinction in the densities between arteries and veins so that they can be distinguished in radiographic analyses. Given that arterial lumina tend to be smaller than venous lumina, the concern arose that arteries might be underdetected using these barium concentrations. As documented below, however, this concern was unwarranted in that arterial visualization was excellent; in fact, small supply vessels had to be digitally "pruned" for the illustrations here to simplify and clarify the vascular tree. About 30 cc each of

the barium-latex solutions were successfully injected into their respective vessels (red for arteries, blue for veins). The particle size of the barium essentially precludes passage of the injection medium through capillary beds, and thus radiographic signals for arteries and veins remain distinct. In the few cases where there was mixing (e.g., within the sinusoids of the paralingual sinuses), this was readily apparent both in the CT scans (intermediate density) and on dissection (purple color). The specimen was refrigerated for several days and refrozen. It was then CT-scanned, dissected, and compared to several osteological specimens of flamingos. For comparison, we also examined injected specimens available in the OUVC of ostrich (*Struthio camelus*), domestic duck (*Anas platyrhynchos*), American alligator (*Alligator mississippiensis*), and green iguana (*Iguana iguana*). These specimens were subjected to CT scanning as well as dissection. Moreover, literally dozens of specimens of birds and reptiles have been dissected by the authors in the past several years, and data from these specimens were consulted.

A pilot CT scan of the flamingo specimen (OUVC 9756) was conducted using a diagnostic scanner (General Electric HiSpeed FX/i helical CT scanner at 1 mm slice thickness, 120 kV, 80 mA) at O'Bleness Memorial Hospital in Athens, Ohio. These test data revealed that that the small size of the specimen necessitated the use of a high-resolution CT scanner to obtain optimal data. CT scanning was performed at the University of Texas High-Resolution X-Ray Computed Tomography Facility at 180 kV and 0.2 mA with 1,000 views per rotation (with two samples averaged per view), an aluminum filter, and an air wedge. The field of view was 73.0 mm across 1,024 $\times$ 1,024 pixel images. Slice thickness and spacing were 0.264 mm (yielding a voxel size of 0.0713 $\times$ 0.0713 $\times$ 0.264 mm, which is highly anisotropic). Reconstruction involved filtered back-projection using the Laks convolution filter. The data were imported into a Dell Precision 360 workstation with 2 GB of RAM and analyzed with Amira 3.1.1 (Mercury-TGS, San Francisco, CA). To ease the handling of the data set, the 16-bit data were converted to 8-bit (256 gray values) and cropped to eliminate extraneous data (e.g., air, uninjected areas of the specimen). The disparities in gray values between injection media, bone, and soft tissue (Fig. 3) were significant enough that the 8-bit data were entirely suitable for our purposes. The data were then resampled using a Lanczos filter to yield a voxel size of 0.12 $\times$ 0.12 $\times$ 0.18 mm. This resampling provided the dual advantage of making the large data set easier to manage and bringing the voxels much closer to isotropy. In order to provide topographic references, the endocranial (brain) cavity and inner ear labyrinths were segmented and rendered in 3D (Fig. 1C and D). A line probe was used in Amira to measure and plot the gray-scale differences between arteries and veins (Fig. 3). The arteries and veins were then segmented based on specified gray-scale values and connectivity. Because of the partial volume effect, a CT artifact that in cross-section creates a penumbra of lower density around the edge of a blood vessel caused by the averaging of the gray-scale values within a single voxel (Fig. 3) (Ketcham and Carlson, 2001), it was necessary to segment some vessels manually as they passed through the more complicated anastomoses to verify accuracy. As a workaround, the area attributed to veins was then swelled, and this larger area was then removed from the artery labels. The segmented arteries, veins, cerebral endocast, inner ear labyrinths, and head were subsequently rendered in 3D (Fig. 1A–D).

The specimen subsequently was dissected under a stereomicroscope to confirm its vascular anatomy (e.g., artery vs. vein, branching pattern), emphasizing anatomy in the orbital, temporal, encephalic, and pharyngeal regions. Thus, all of the CT-based visualizations illustrated here have been validated by gross observation. Although it would have been advantageous to have had an injection/dissection sample larger than this single individual, the anatomical, radiographic, and analytical approaches are so labor-intensive that a larger sample would have been impractical. This problem was ameliorated by identifying key osteological correlates for known vascular structures, thus expanding the sample by including dried skull specimens of *P. ruber* [e.g., Stony Brook University (SBU) 107161], as well as other flamingo species such as *P. minor* [Field Museum of Natural History (FMNH) 108183, OUVC 9757, 9758]. These specimens were scored for the presence of specific bony foramina, canals, grooves, and fossae associated with the vessels observed in the injected fleshy specimen (OUVC 9756); many of these same bony features are widely distributed in birds (Baumel and Witmer, 1993).

RESULTS

CT scanning, image analysis, and dissection all reveal that the overall vascular pattern of flamingos (Figs. 1A, B, and F, 2, 4, and 5) closely resembles that of other birds, confirming that avian cephalic vasculature is evolutionarily conservative. Several vascular plexuses are present in the orbitotemporal (e.g., rOP; Fig. 1E), suborbital (e.g., vMX; Fig. 1E), and nasal (e.g., plCH; Fig. 1A and B) regions. In addition, vessels from the pharyngeal, suborbital, and submandibular regions reach the rictus (corner of the mouth), contributing blood flow to structures such as the Harderian gland, palatal plexus, pharyngeal mucosa (Fig. 1F), and rhamphotheca. Moreover, we discovered a pair of novel paralingual vascular sinuses or cavernous tissue masses. Vascular nomenclature generally follows Baumel (1993) and Sedlmayr (2002). The following description generally proceeds in a caudal-to-rostral direction beginning near the occiput.

Overview of Cephalic Vasculature

The primary trunks of the common carotid artery (aCC) are easily identifiable, although smaller neighboring tertiary branches are more difficult to discern because of the complexity of the vascular trees. The first major dorsal branches of the common carotid artery include the internal (cerebral) carotid (aCI) and stapedial (external ophthalmic; aST) arteries, both of which pass through the tympanic cavity (Fig. 4B). The internal carotid artery anastomoses with the palate via the sphenopalatine (aSP) and sphenomaxillary arteries (Fig. 1D), the basilar artery via the caudal encephalic artery (aEU; Fig. 1C), and the orbit via the ethmoidal (aET) and cerebral ophthalmic arteries (Fig. 1B). As in many other birds (Baumel and Gerchman, 1968), there is an extensive internal carotid anastomosis lying within the carotid canal, prior to the entrance into the hypophyseal fossa. The stapedial artery

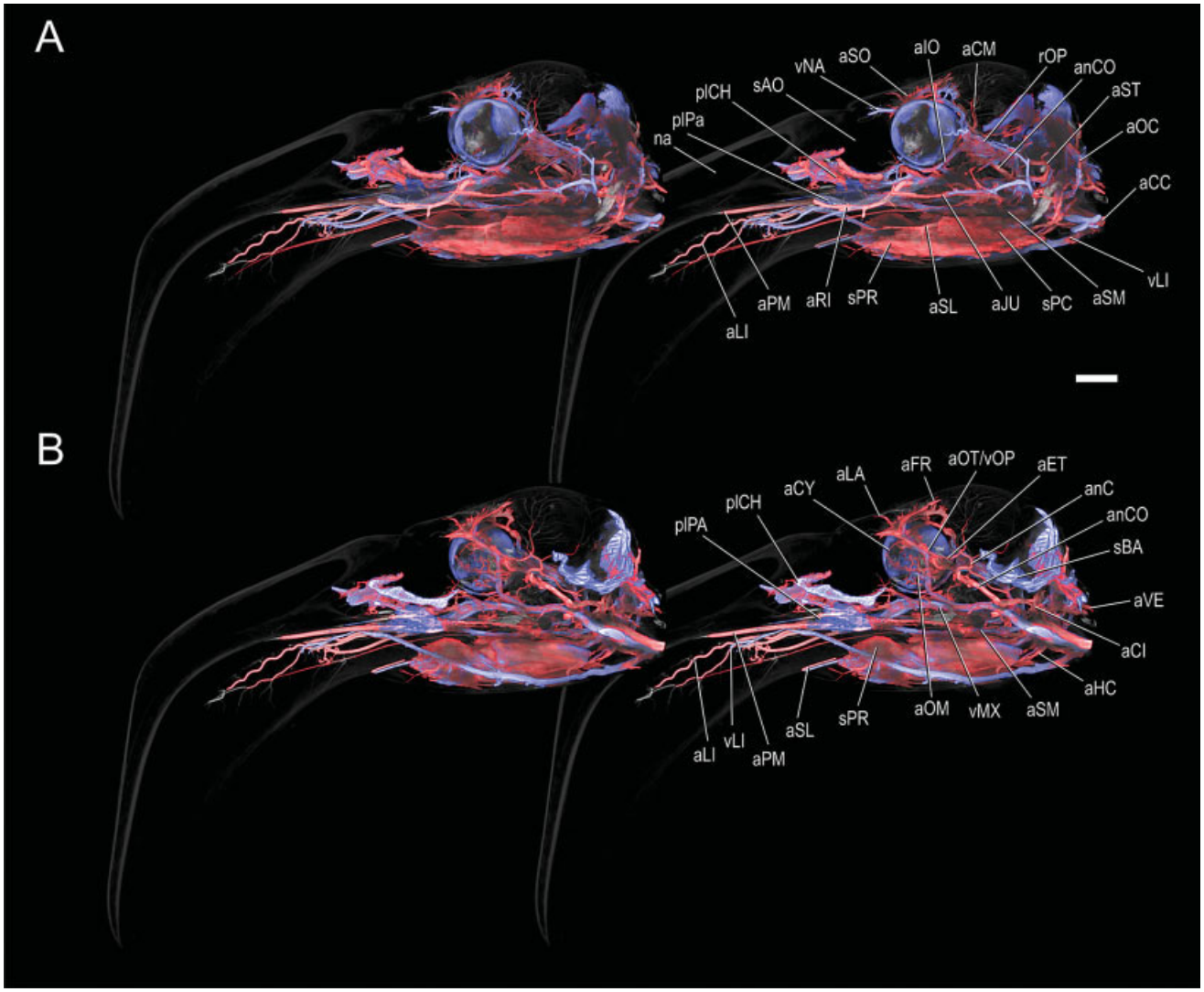

Fig. 1. The cephalic vasculature and relevant anatomical structures of the Caribbean flamingo (*Phoenicopterus ruber*; OUVC 9756) using vascular injection, CT imaging, segmentation analysis, and dissection. Stereopairs. **A:** Left lateral view. **B:** Medial view of right side of midsagittal section. **C:** Right dorsolateral oblique view of cranial region with endocasts of brain cavity (semitransparent), osseous labyrinth of inner ear (yellow), and encephalic and orbitotemporal vessels. **D:** Left, dorsal, and slightly lateral view of the same structures as in C. Dissections (see insets for orientation). **E:** Temporal and orbital region in right lateral view. **F:** Pharyngeal and paralingual region in right ventral oblique view with tissues ventrally retracted from mandible. Scale bars = 10 mm.

supplies most of the temporal and orbital regions of the head, including the ophthalmic rete (rOP) via the lateral temporal artery, jaw muscles via the superficial temporal artery (aTS; Fig. 1E), the orbit via the profundus artery and its bulbar branches, and the supraorbital salt glands via the supraorbital artery (aSO; Fig. 1A). The occipital artery (Fig. 1A) branches from the stapedial artery near the caudal part of the middle ear cavity. This relationship is similar to that found in herring gulls (*Larus argentatus*) (Midtgård, 1984b) and cormorants (*Phalacrocorax auritus*; personal observation), where it also branches from the stapedial artery, although closer to the rostral part of the middle ear. However, this pattern differs from the one found in *Anas platyrhynchos* (Sedlmayr, 2002), where the occipital artery branches from the internal carotid artery caudal to the middle ear cavity, and *Gallus gallus*, where the artery arises from the external carotid artery (Baumel, 1975). The occipital artery in flamingos and other birds then passes through a bony canal within the diploe of the skull to exit into the dorsal portion of the epaxial cervical musculature.

Ventrally, the caudal hyoidal (aHC) and hyolingual arteries branch from the common carotid artery and supply throat and hyolingual structures, sending both caudal and rostral branches into the oropharyngeal viscera (Fig. 1F). The lingual (aLI) and submandibular (aSM) arteries branch off the hyolingual artery and course rostrally into the tongue and the lateral wall of the pharynx, respectively (Figs. 1B and F and 2A and C). The submandibular artery supplies the highly vascular pharyngeal wall as a complex arteriovenous rete. It eventually anastomoses with the maxillary vein and with the pterygoid, spheno-

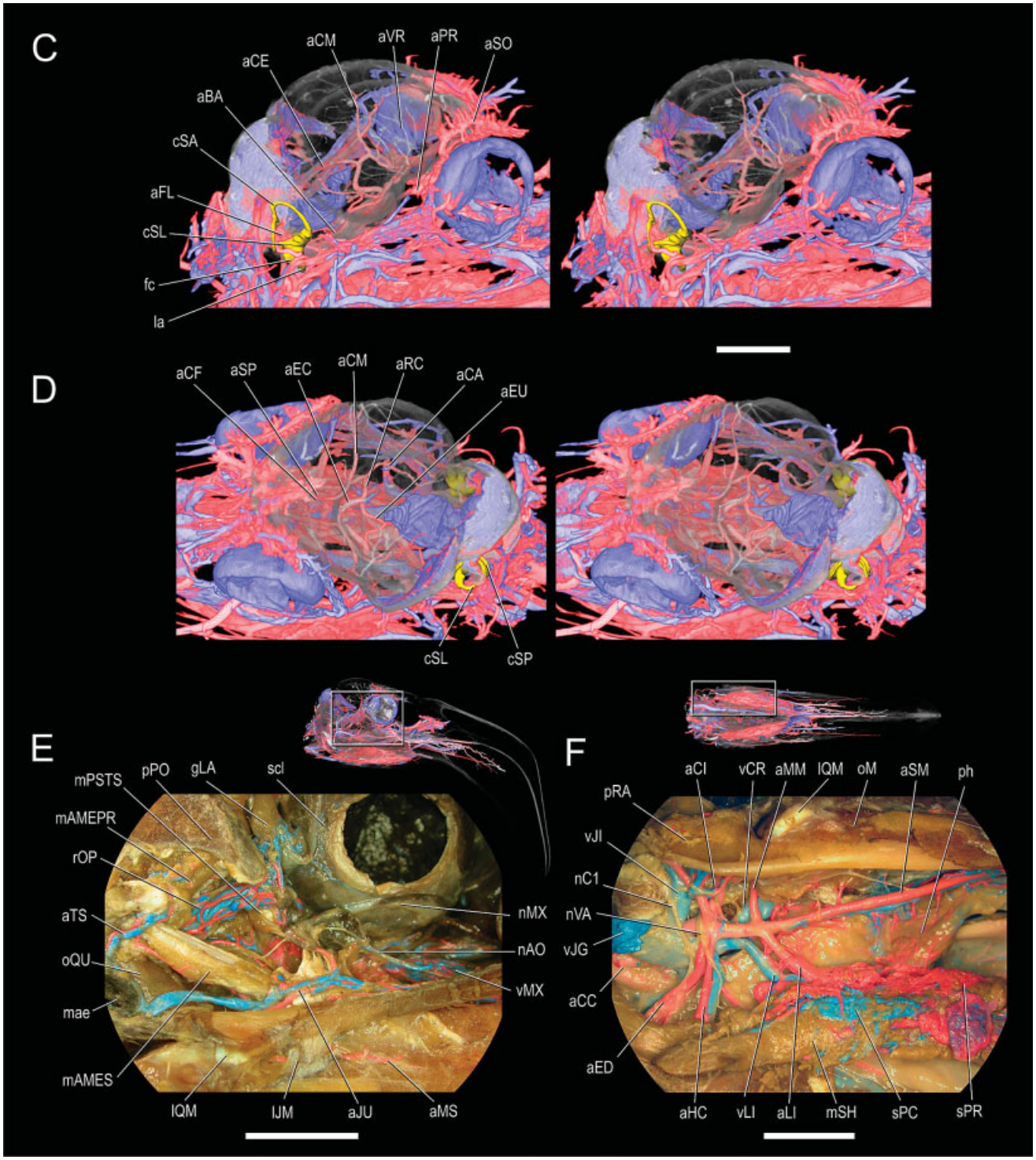

Fig. 1. (Continued)

palatine, and jugal arteries at the rictus of the mouth and contributes to the palatal plexus (Figs. 1A and 4B). The external carotid artery continues rostrally as the temporomandibular artery, which ramifies into the pterygoid, jugal (aJU), and mandibular (aMN) arteries (Figs. 1A and 4B). These vessels anastomose with numerous other vessels from the submandibular, sphenopalatine, and sphenomaxillary arteries along the lateral aspect of the orbit and palate.

The cerebral arterial circle is visible within the endocranial cavity (Fig. 1D). The basilar artery splits into the paired caudal encephalic arteries (aEU), each of which

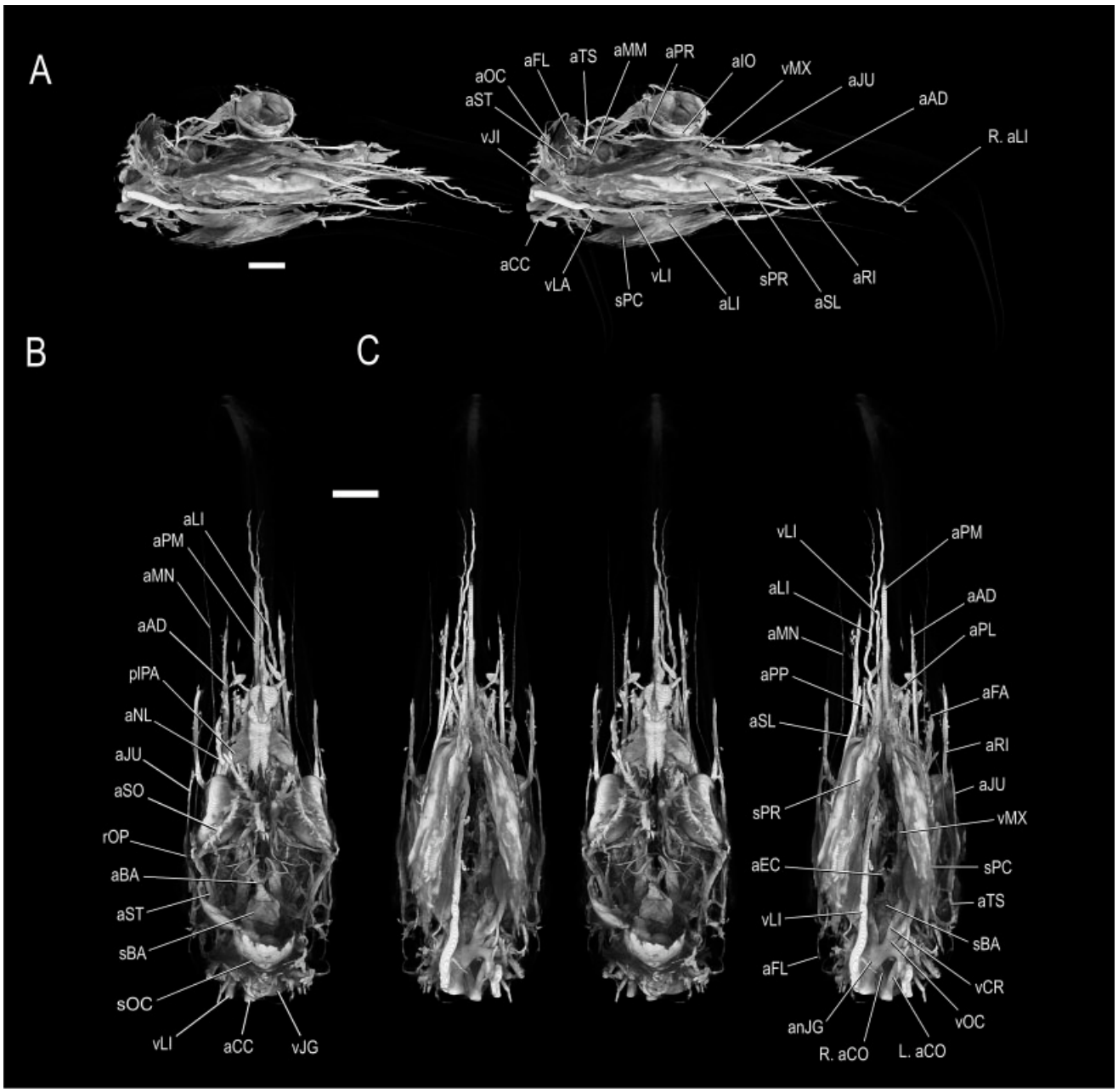

Fig. 2. Stereopairs of segmented flamingo cephalic vasculature. **A:** Right ventral oblique view. **B:** Dorsal view. **C:** Ventral view. Scale bars = 10 mm.

anastomoses with the ipsilateral common encephalic artery (aEC). The common encephalic artery, the terminal branch of the internal carotid artery, branches into the common rostral cerebral (aRC) and caudal cerebral arteries (aCA; Fig. 1D). The common rostral cerebral subsequently branches into the frontal cerebral (aCF), ethmoid (aET), and cerebral ophthalmic arteries (Fig. 1B). The caudal portions of the dural venous sinuses are present and likely overinflated in the occipital region of the cranial cavity. Just rostroventral to the dural sinuses, the basilar plexus (plBA) is formed by the basilar artery and the anastomoses of the jugular veins (Fig. 1B and D). Although not well visualized in the scan data, the caudal cerebral artery arises from the right common encephalic artery, a common asymmetry present among avian taxa (Baumel, 1967).

The palatal vessels (sphenopalatine medially, sphenomaxillary laterally) exit the cranial base along the basisphenoid and pterygoid bones. These vessels form dense vascular plexuses with the large maxillary vein and their contralateral counterparts in the suborbital region (e.g., Harderian gland) and palatal mucosa (e.g., palatal plexus). From these plexuses, the sphenopalatine artery anastomoses with the nasal branches of the ethmoid ar-

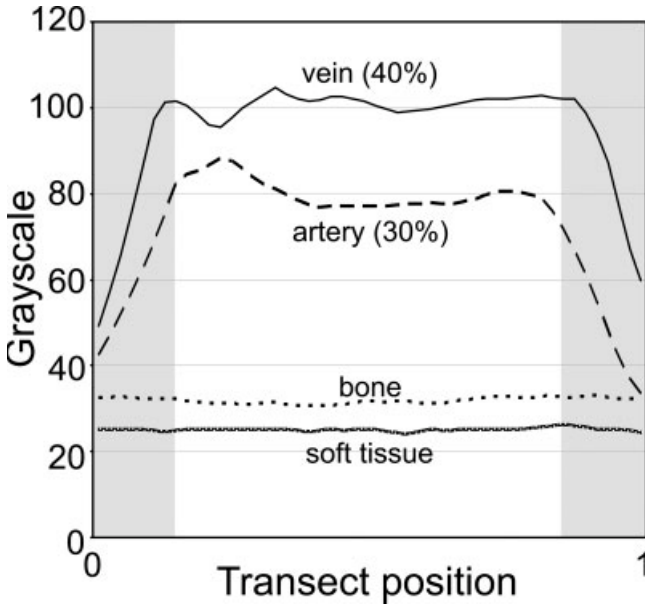

Fig. 3. Distribution of 8-bit gray-scale (X-ray attenuation) values of CT data along transects perpendicular to the injected jugular vein (solid line), injected common carotid artery (dashed line), dense cortical bone (dotted line), and soft tissue of the tongue (hatched line). The transect lengths were standardized to allow direct comparison. Gray boxes at the sides represent partial volume averaging at the edges of the injected vasculature. Percentages for the vein and artery reflect the amount of barium in the barium/latex injection medium. The minimal overlap in gray-scale values of these structures allows their discrimination and segmentation within the CT data.

tery as part of the caudal and middle conchal plexuses (plCH) of the nasal cavity (Fig. 4A) and then combines with its contralateral counterpart to form the median palatine artery (aPM), which courses rostrally along the midline of the palate (Figs. 1A and 4A). The sphenomaxillary artery anastomoses laterally with the facial and dorsal alveolar branches of the temporomandibular artery to form the antorbital vascular plexus around the antorbital air sinus.

Accompanying the arteries are numerous veins, several of which are anatomically significant. For example, the palatine, rictal, dorsal alveolar, and nasal veins all drain the numerous vascular plexuses of the orbitonasal region of the head. These vessels and the ophthalmic vein from the eye drain into the large maxillary vein (vMX), which courses along the dorsal surface of the pterygoid (Fig. 2C). The maxillary vein merges with the temporomandibular vein (which drains the ophthalmic rete and mandible), forming the rostral cephalic vein (vCR), which then merges with the sphenopalatine and sphenomaxillary veins along the ventral aspect of the braincase (Fig. 2C). The lingual vein is the last cephalic contribution to the large bijugular anastomosis that lies alongside the common carotid artery at the craniocervical junction.

Paralingual Sinuses

A pair of novel paralingual sinuses were discovered upon CT imaging (Figs. 1, 2, 4, 5, 6, and 7). The sinuses clearly are not an artifactual "blow out" because they are bilaterally symmetrical and have a characteristic vascular architecture, as confirmed by dissection. The sinuses are large enough in the injected specimen (OUVC 9756) to excavate a large ovate bony depression on the medial surface of the lower jaw, just ventral to the medial mandibular fossa and rostral to the medial mandibular process and the insertion of the pterygoideus musculature (Fig. 6A and B). This medial depression is apparently a consistent and highly reliable osteological correlate of the paralingual sinus in that similar fossae were identified in the skulls of other *P. ruber* specimens (e.g., SBU 107161), as well as skulls of other flamingo species (e.g., *P. minor*: FMNH 108183, OUVC 9757, 9758; Fig. 6C). Moreover, fossae on the inner surface of the mandible that could potentially be confused with the paralingual sinus fossa, such as those for jaw muscles and the mandibular neurovascular bundle, are well understood (Holliday, 2006) and can be shown to be separate from the paralingual sinus fossa (Fig. 6). Turning to potentially related taxa such as anseriforms and ciconiiforms (Fig. 6D and E) as well as the basal avian taxon *Struthio* (Fig. 6F), although all relevant muscular attachments and neurovascular fossae can be identified in these taxa, none bears a fossa similar to the paralingual sinus fossa of flamingos. Likewise, no such vascular sinus has been found in our dissections of birds other than flamingos.

The paralingual sinuses are located anatomically between the ipsilateral serpihyoideus muscle (mSH) (Vanden Berge and Zweers, 1993) and ceratohyal ventrolaterally (Fig. 1F), the pterygoideus ventralis muscle (mPTV; Fig. 6) and pharyngeal mucosa dorsomedially, the trachea, laryngeal artery, laryngopharynx, and tongue medially, and the lower jaw rostrolaterally (Figs. 1, 2, 4, and 5). Each sinus is suspended between the lingual artery (a large branch of the hyolingual artery) dorsomedially and lingual vein ventromedially (Figs. 1 and 2A). The lingual vein invests the ventromedial portion of the sinus and drains caudally into the jugular vein on the right side and into the rostral cephalic vein on the left side. Each sinus can be divided into two fairly discrete lobes, a caudolateral lobe (sPC) and a rostromedial (sPR) lobe connected by a thin isthmus of glandular tissue (Figs. 4B, C, and G, 5A and B, and 7). The sublingual artery (aSL) branches off from the lingual artery just dorsal to the caudal portion of the caudolateral paralingual lobe and runs rostrolaterally between the two paralingual lobes, where it continues rostrally as a helicine artery along the lateral sides of the basihyale and paraglossus muscles of the tongue (Homberger, 1988). The left sinus is primarily arterial, whereas the right sinus is partitioned into a venous portion in the caudolateral lobe and an arterial and mixed (i.e., purple latex) region in the rostromedial lobe (Fig. 1F). A large laryngeal artery that supplies the laryngopharynx branches off the lingual artery dorsomedially within the rostromedial lobe of the paralingual sinus. The lingual artery then continues into the distal end of the tongue, where it ends in a dense lingual plexus.

DISCUSSION

Flamingos share a number of similar vascular patterns with other birds, including an asymmetrical cau-

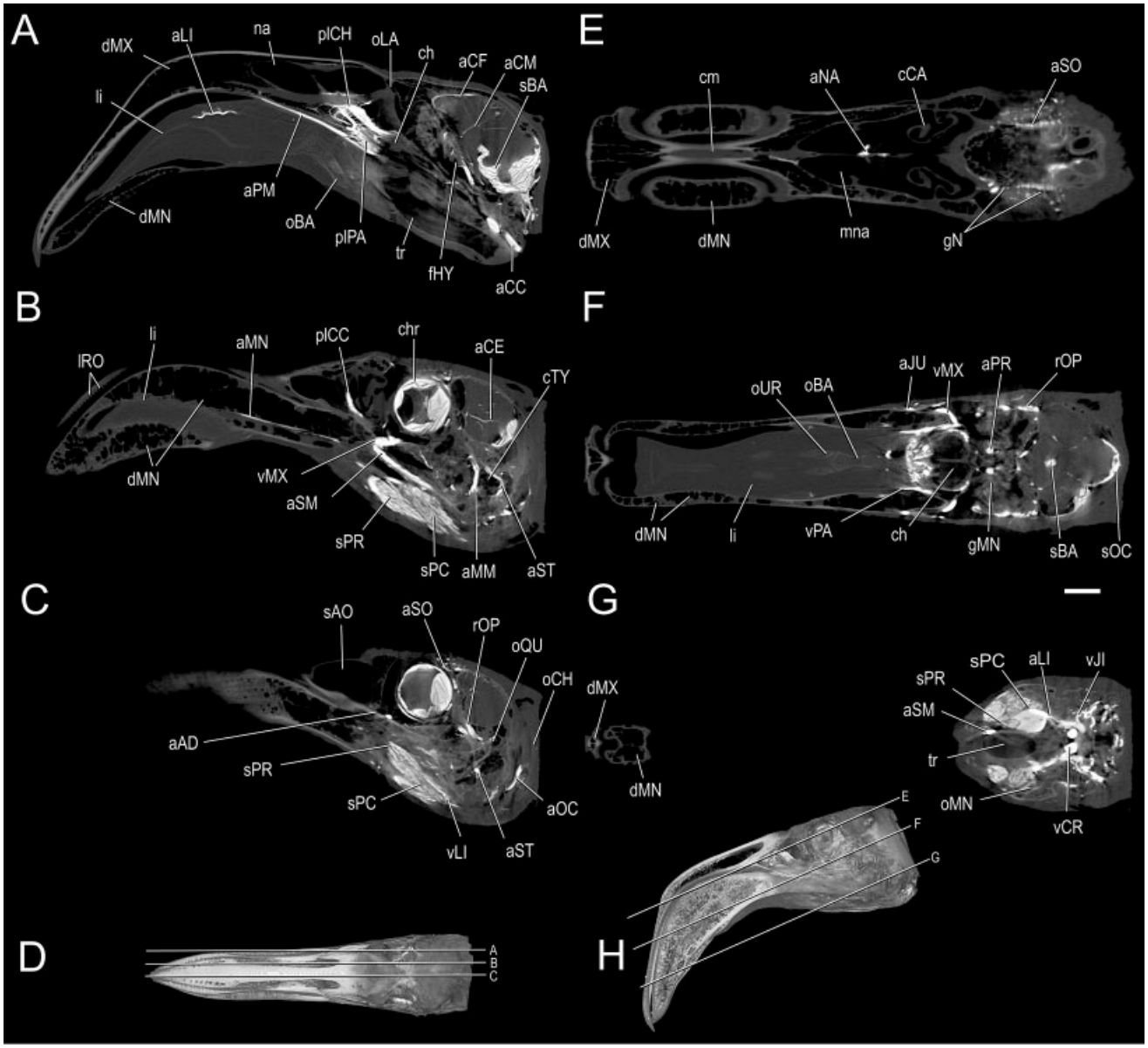

Fig. 4. Representative slices through CT data of flamingo head. **A–C:** Parasagittal sections. **D:** Dorsal image of head depicting location of parasagittal slices in A–C. **E–G:** Horizontal sections. **H:** Lateral image of head depicting location of horizontal slices in E–G. Scale bar = 10 mm.

dal cerebral artery and a complex assortment of vascular devices (e.g., the ophthalmic rete). However, particular differences in the branching patterns of some vessels, such as the occipital artery, may eventually shed light on resolving the relatively ambiguous taxonomic relationship flamingos share with other avian groups. In addition, this study revealed the presence of an unanticipated and previously undescribed vascular device, the paralingual sinus. The new vascular injection protocols used here hold promise as a means of distinguishing and then visualizing the three-dimensional anatomy of arteries and veins in CT data sets. This approach successfully demonstrates and, for the first time, allows documentation of the arterial and venous patterns of flamingo head vessels. It is an important advantage to be able to study and analyze all of the vascular plexuses and devices in the virtual realm prior to engaging in destructive and yet ultimately valuable dissection.

Techniques aside, the paralingual sinuses themselves are intriguing structures. They clearly are vascular devices, yet their function has not been experimentally tested. In general, arterial blood supplies the sinuses via the hyolingual system (lingual and sublingual arteries), and the sinuses are drained via the lingual vein. The caudolateral lobes are tightly interwoven with the serpihyoideus muscle, a strap muscle of the hyoid skeleton. Ostensibly glandular material (nonmuscular, nonvascular tissue) also permeates the caudolateral lobe, whereas

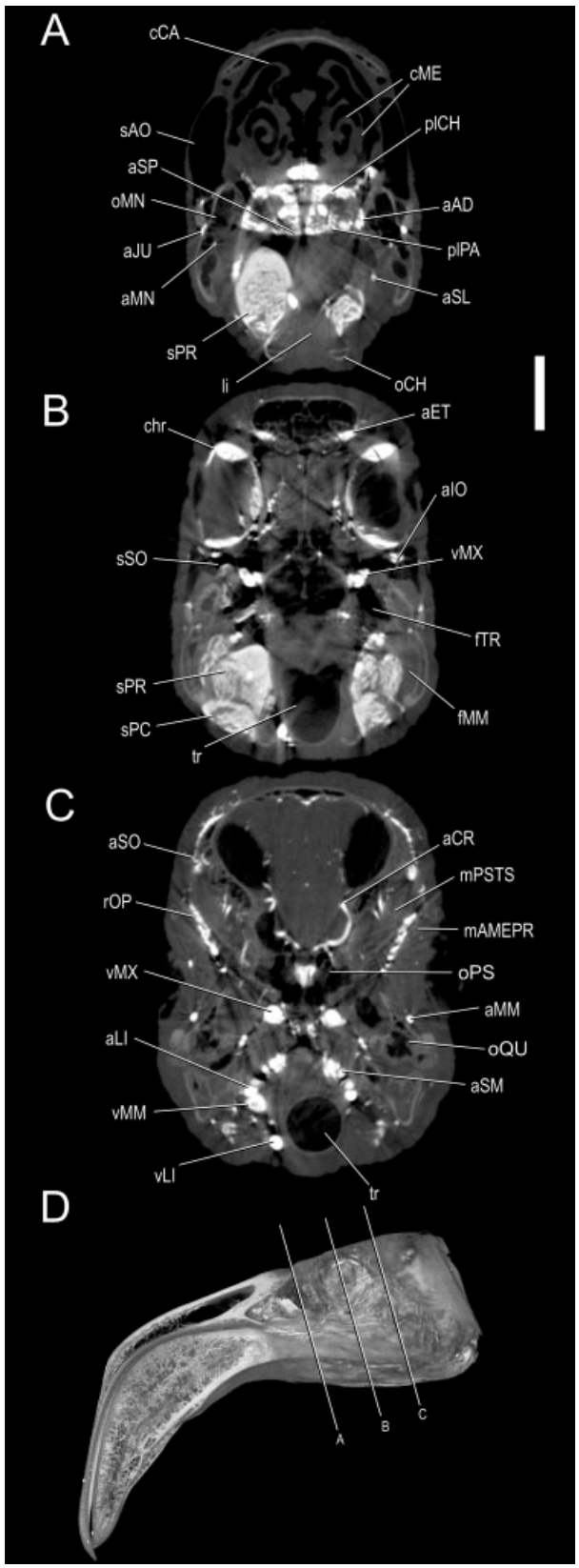

Fig. 5. Representative axial (coronal) slices through CT data of flamingo head. **A–C:** Slices. **D:** Lateral image of head depicting location of axial slices in A–C. Scale bar = 10 mm.

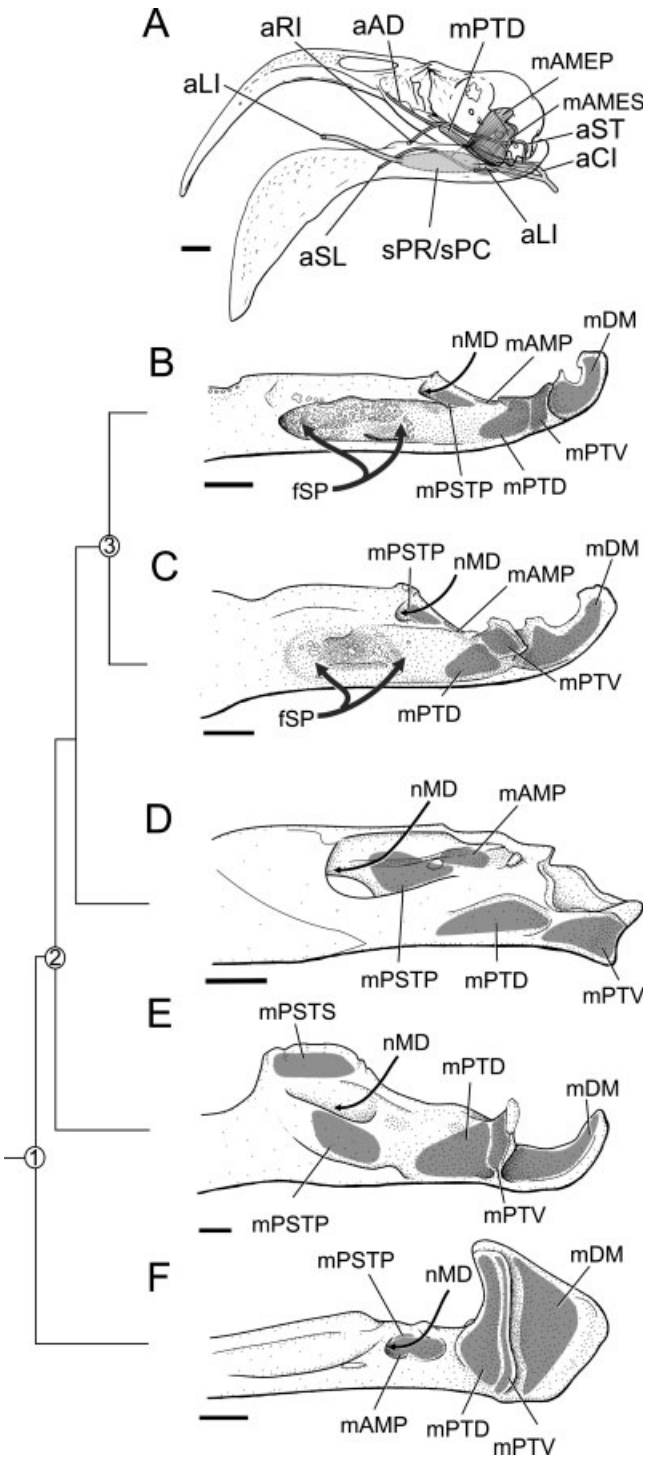

Fig. 6. Osteological correlates of the paralingual vascular sinus of flamingos and its relationship to the lower jaw and adductor musculature compared to other, potentially related avian taxa. **A:** Schematic illustrating general orientation of sinus, major vessels, and musculature. **B–F:** Lower jaws in right medial view of (B) *Phoenicopterus ruber* (Caribbean flamingo, OUVC 9756); (C) *Phoenicopterus minor* (lesser flamingo, OUVC 9758); (D) *Ephippiorhynchus asiaticus* (black-necked stork; FMNH 378508); (E) *Anser anser* (domestic goose, OUVC 10214); (F) *Struthio camelus* (ostrich, OUVC 9592). Nodes: 1, Neornithes; 2, Neognathae; 3, Phoenicopteridae. Scale bars = 10 mm.

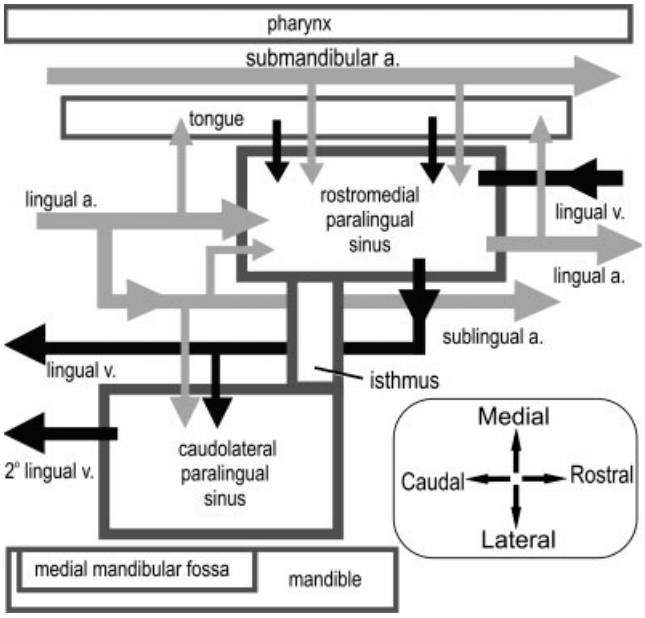

Fig. 7. Diagram illustrating right paralingual sinus, its vascular supply, and relevant surrounding structures in dorsal view.

the rostromedial lobe is almost completely vascular and surrounds the lingual artery. Based on this anatomical arrangement, possible functional hypotheses include a secondary salinity regulatory structure (the primary excretory organ of the head being the supraorbital salt glands, the vasculature of which also is visible on this scan); a countercurrent heat exchanger [e.g., as part of the circumpharyngeal vascular ring (Baumel et al., 1983; Arad et al., 1989; Sedlmayr, 2002)]; and, perhaps most likely, a cavernous mass of erectile tissue providing a mechanical adjunct to the peculiar lingual-pump feeding mechanism by allowing controlled adjustment (via variable engorgement) of mechanical stiffness of the system. Whatever the specific role of the vascular device [see Midtgård (1984a) and Sedlmayr (2002) for elaboration on avian vascular devices], its association with the quickly pumping hyolingual system and its proximity and vascular communication with the jaw muscles, pharynx, and lower jaw (all of which likely physically constrain the sinus) certainly indicate the importance of this previously unknown device and merits further investigation.

ACKNOWLEDGMENTS

The authors thank Tobin Hieronymus and Lisa Cooper for assistance with the injection; Heather Mayle and O'Bleness Memorial Hospital, Athens, Ohio, as well as Richard Ketcham, Matthew Colbert, and Timothy Rowe at the University of Texas at Austin's High-Resolution CT Facility for providing access to and technical assistance with CT scanning; Julian Humphries for assisting with the accompanying Web site on DigiMorph.org; Chris DeLorey (Brevard Zoo) for donation of the specimen; and Hauke Bartsch (Template Graphics Software) for providing helpful suggestions for approaching the CT data. Funding was provided by NSF grants to L. M. Witmer (Ohio University) and to T. Rowe (University of Texas), and by Ohio University and the College of Osteopathic Medicine.

LITERATURE CITED

Arad Z, Midtgård U, Bernstein MH. 1987. Posthatching development of the rete ophthalmicum in relation to brain temperature of mallard ducks (*Anas platyrhynchos*). Am J Anat 179:137–142.

Arad Z, Midtgård U, Bernstein MH. 1989. Thermoregulation in turkey vultures: vascular anatomy, arteriovenous heat exchange, and behavior. Condor 91:505–514.

Baumel JJ. 1967. The characteristic asymmetrical distribution of the posterior cerebral artery of birds. Acta Anat 67:523–549.

Baumel JJ, Gerchman L. 1968. The avian intercarotid anastomosis and its homologue in other vertebrates. Am J Anat 122:1–18.

Baumel JJ. 1975. Aves: Heart and blood vessels. In: Getty R, editor. Sisson and Grossman's the anatomy of the domestic animals. Philadelphia, PA: W.B. Saunders. p 1968–2003.

Baumel JJ, Dalley AF, Quinn TH. 1983. The collar plexus of subcutaneous thermoregulatory veins in the Pigeon, *Columba livia*: its association with esophageal pulsation and gular flutter. Zoomorphology 102:215–239.

Baumel JJ. 1993. Systema cardiovasculare. In: Baumel JJ, editor. Handbook of avian anatomy: nomina anatomica avium. Cambridge, MA: Nuttall Ornithological Club. p 407–476.

Baumel JJ, Witmer LM. 1993. Osteologia. In: Baumel JJ, editor. Handbook of avian anatomy: nomina anatomica avium. Cambridge, MA: Nuttall Ornithological Club. p 45–132.

Clifford AB, Witmer LM. 2004. Case studies in novel narial anatomy, II: the enigmatic nose of moose (Artiodactyla: Cervidae: *Alces alces*). J Zool 262:339–360.

Crowe TM, Crowe AA. 1979. Anatomy of the vascular system of the head and neck of the helmeted guinea fowl *Numida meleagris*. J Zool 188:221–233.

Feduccia A. 1976. Osteological evidence for shorebird affinities of the flamingos. Auk 93:587–601.

Feduccia A. 1978. Presbyornis and the evolution of ducks and flamingos. Am Sci 66:298–304.

Hagey LR, Schteingart CD, Ton-Nu H-T, Rossi SS, Odell D, Hofmann AF. 1990. β-phocacholic acid in bile: biochemical evidence that the flamingo is related to an ancient goose. Condor 92:593–597.

Holliday CM. 2006. Evolution of the adductor chamber in Archosauria: topology, homology, and function in crocodilians, dinosaurs, and birds. PhD dissertation. Athens, OH: Ohio University.

Homberger DG. 1988. Comparative morphology of the avian tongue. In: Oeullet H, editor. Acta XIX congressus internationalis ornithologici, vol. 2. Ottawa: University of Ottawa Press. p 2427–2435.

Jenkin PM. 1957. The filter-feeding and food of flamingoes (Phoenicopteri). Phil Trans R Soc Biol 240:401–493.

Kaku K. 1959. On the vascular supply of the brain in the domestic fowl. Fukuoka Acta Med 50:4293–4306.

Ketcham RA, Carlson WD. 2001. Acquisition, optimization and interpretation of X-ray computed tomographic imagery: applications to the geosciences. Comp Geosci 27:381–400.

Mascitti V, Kravetz FO. 2002. Bill morphology of South American flamingos. Condor 104:73–83.

Mayr G, Clarke J. 2003. The deep divergences of neornithine birds: a phylogenetic analysis of morphological characters. Cladistics 19:527–553.

Mayr G. 2004. Morphological evidence for sister group relationship between flamingos (Aves: Phoenicopteridae) and grebes (Podicipedidae). Zool J Linn Soc 140:157–169.

Midtgård U. 1984a. Blood vessels and the occurrence of arteriovenous anastomoses in cephalic heat loss areas of mallards, *Anas platyrhynchos*, Aves. Zoomorphology 104:323–335.

Midtgård U. 1984b. The blood vascular system in the head of the herring gull (*Larus argentatus*). J Morphol 179:135–152.

Olsen SL, Feduccia A. 1980. Relationships and evolution of flamingos (Aves: Phoenicopteridae). Smith Contr Zool 316:1–73.
Richards SA. 1967. Anatomy of the arteries of the head in the domestic fowl. J Zool 152:221–234.
Richards SA. 1968. Anatomy of the veins of the head in the domestic fowl. J Zool 154:223–234.
Sedlmayr JC. 2002. Anatomy, evolution, and functional significance of cephalic vasculature in Archosauria. PhD dissertation. Athens, OH: Ohio University.
Sedlmayr JC, Witmer LM. 2002. Rapid technique for imaging the blood vascular system using stereoangiography. Anat Rec 267:330–336.
Sibley CG, Ahlquist JE. 1990. Phylogeny and classification of birds—a study in molecular evolution. New Haven, CT: Yale University Press.
Vanden Berge, JC, Zweers GA. 1993. Myologia. In: Baumel JJ, editor. Handbook of avian anatomy: nomina anatomica avium. Cambridge, MA: Nuttall Ornithological Club. p 189–247.
van Tuinen MD, Butvill B, Kirsch JAW, Hedges SB. 2001. Convergence and divergence in the evolution of aquatic birds. Proc R Soc Lond B 268:1345–1350.
Witmer LM. 2001. Nostril position in dinosaurs and other vertebrates and its significance for nasal function. Science 293:850–853.
Zweers GA, Berkhoudt H, Vanden Berge JC. 1994. Behavioral mechanisms of avian feeding. In: Bels VL, Chardon M, Vandewalle P, editors. Biomechanics of feeding in vertebrates. Berlin: Springer-Verlag. p 241–279.
Zweers GA, de Jong F, Berkhoudt H. 1995. Filter feeding in flamingos (*Phoenicopterus ruber*). Condor 97:297–324.